Chinese Chemical Letters 34 (2023) 108531

Contents lists available at ScienceDirect

Chinese Chemical Letters

journal homepage: www.elsevier.com/locate/cclet

Topological effect on fluorescence emission of tetraphenylethylene-based metallacages☆

Yuhang Liu[a,b,1], Zhewen Guo[a,b,1], Yuchen Guo[b], Guangfeng Li[b], Shengbing Yang[c], Xuzhou Yan[b,*], Yi Shen[a,*], Jinbing Wang[a,*]

[a] Department of Oral and Maxillofacial-Head and Neck Oncology, Shanghai Ninth People's Hospital, Shanghai Jiao Tong University School of Medicine, College of Stomatology, National Center for Stomatology, National Clinical Research Center for Oral Diseases, Shanghai Key Laboratory of Stomatology, Shanghai Jiao Tong University, Shanghai Research Institute of Stomatology, Shanghai 200011, China
[b] School of Chemistry and Chemical Engineering, Frontiers Science Center for Transformative Molecules, Shanghai Jiao Tong University, Shanghai 200240, China
[c] Shanghai Key Laboratory of Orthopaedic Implants, Department of Orthopaedic Surgery, Shanghai Ninth People's Hospital, Shanghai Jiao Tong University School of Medicine, Shanghai 200125, China

ARTICLE INFO

Article history:
Received 18 December 2022
Revised 23 April 2023
Accepted 27 April 2023
Available online 30 April 2023

Keywords:
Topological effect
Photophysical properties
Aggregation-induced emission
Coordination-driven self-assembly
Supramolecular metallacages

ABSTRACT

Herein, we describe the selective formation of a barrel-shaped or a ball-shaped fluorescent metallacage by controlling the shape and stoichiometry of the building blocks. Specifically, the tetraphenylethylene-based donor and two acceptors with different numbers of Pt(II) centers were combined *via* coordination-driven self-assembly. Owing to the differences in the shapes of the assemblies, the resultant ball-shaped metallacage displayed stronger and blue-shifted fluorescence compared to the barrel-shaped one in dilute solutions, while a reversal of fluorescence intensities was observed in the aggregation process. Overall, this work demonstrates that the photophysical properties of supramolecular coordination complexes can be affected by subtle geometrical factors, which can be controlled precisely at the molecular level.

Fluorescent materials have attracted widespread research interest in recent decades on account of their promising applications in light-emitting diodes, biological sensing, organic electronic devices and so on [1–4]. Nevertheless, conventional organic fluorophores generally showcase weakened or entirely quenched emission in condensed states owing to the aggregation-caused quenching (ACQ) effects, which vastly restricts their applications in necessary high concentration or solid state [5–7]. This puzzle was tactfully tackled when Tang and co-workers reported an inverse phenomenon known as aggregation-induced emission (AIE) [8,9]. Specific fluorophores are almost non-emissive in dilute solution yet display brilliant emission under aggregation states due to the astriction of intramolecular rotation [10,11]. Tetraphenylethylene (TPE) is the most representative AIE-active fluorophore whose free rotation of phenyl rings and twisting of the C=C bond are astricted in aggregative states, thereby suppressing the nonradiative decay and allowing efficient emission [12–14]. Due to the distinct optical behavior and facile modification, TPE fluorogens have been extensively introduced into organic frameworks, polymeric materials, and supramolecular assemblies to regulate their photophysical properties and facilitate the development of various intriguing fluorescent materials [15–20]. Fundamentally, the emission of TPE fluorophores is highly correlated to the degree of conformational distortion [21,22]. However, study on the relationship between fine structures of TPE-based fluorescent materials and the accompanying emissive behaviors represents a significant challenge.

Coordination-driven self-assembly *via* the spontaneous formation of metal−ligand bonds can provide a powerful strategy for addressing the scientific issue above [23–26]. In this strategy, the self-assembly between the Lewis-basic donor and Lewis-acidic acceptor can go through efficient error correction and self-repairing process benefiting from their kinetic reversibility, thereby resulting in thermodynamically favorable supramolecular coordination complexes (SCCs) with predictable shapes and sizes [27,28]. As a kind of representative SCCs, discrete metallacages could have the well-defined three-dimensional geometry and conformation through regulating the angularity, size and stoichiometry of the rigid precursors, which are emerged as a promising platform to investigate AIE properties [29,30]. As such, the TPE fluorogens could be incorporated into well-designed metallacages to adjust their

☆ Dedication to Prof. Lixin Dai on the Occasion of His Centenary Birthday.

* Corresponding authors.
E-mail addresses: xzyan@sjtu.edu.cn (X. Yan), SHENYI1866@sh9hospital.org.cn (Y. Shen), 118030@sh9hospital.org.cn (J. Wang).

[1] These authors contributed equally to this work.

https://doi.org/10.1016/j.cclet.2023.108531
1001-8417/

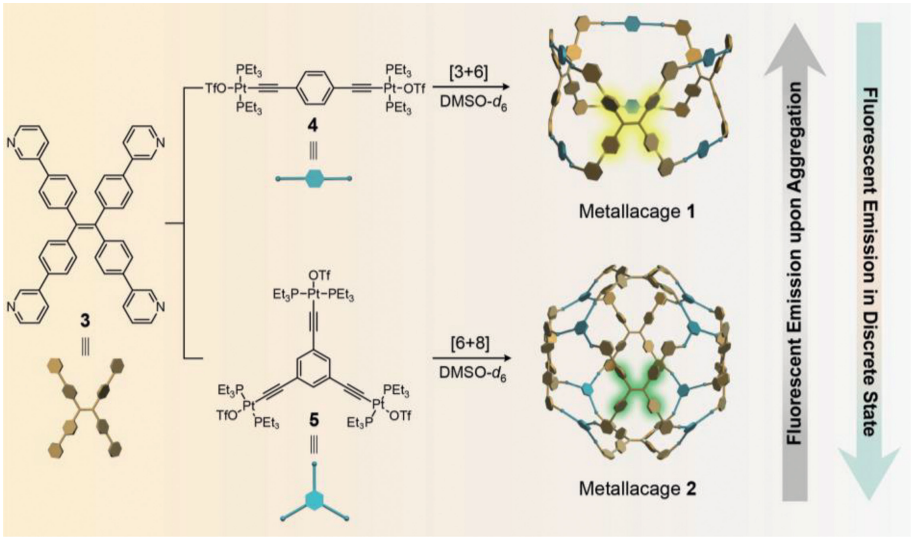

Fig. 1. Schematic representation of the formation of the metallacages **1** and **2** with different topological structures and photophysics *via* coordination-driven self-assembly.

topological conformation, therefore leading to variable fluorescent properties. Although a wealth of delicate TPE-based emissive SCCs have been reported, the influence of topological geometries on fluorescent behavior is rarely investigated [31–33]. In coordination-driven self-assembly, subtle change of building blocks generally results in SCCs with different geometries [34,35]. Therefore, we envision that such SCCs can serve as an ideal model system to explore the impacts of fine structures and geometrical effect of TPE-based fluorescent materials on their emissive behaviors.

Herein, we designed and synthesized two TPE-based metallacages, **1** and **2**, with different topological geometries *via* the coordination-driven self-assembly, and further investigated the emissive behaviors of TPE in the distinguishing fine structures (Fig. 1). In specific, the TPE-based tetrapyridyl ligand **3** was selected to coordinate with the di-Pt(II) acceptor **4** in a 3:6 ratio to form a barrel-shaped metallacage **1**, and with the tri-Pt(II) acceptor **5** in a 6:8 ratio to yield a ball-shaped metallacage **2**, respectively. With the same donor, we obtain two metallacages with distinct geometries by varying the metal acceptors. Notably, the different topological conformations lead to variable emissive properties of the two metallacages in spite of possessing identical TPE core.

In this work, we combined the TPE-based tetrapyridyl ligand **3** with the di-Pt(II) acceptor **4** and tri-Pt(II) acceptor **5**, respectively, to fabricate two different TPE-containing metallacages with the barrel-shape or ball-shape (Fig. 1). In detail, by mixing the ligand **3** and di-Pt(II) acceptor **4** in a 3:6 ratio at 70 °C for 8 h in deuterated DMSO, the barrel-shaped metallacage **1** was obtained in nearly quantitative yield. Meanwhile, the ball-shaped metallacage **2** was prepared *via* the self-assembly between the ligand **3** and tri-Pt(II) acceptor **5** in a 6:8 ratio by following the same synthetic method.

The formation of these two discrete TPE-containing metallacages was first investigated by NMR analyses (^{1}H and ^{31}P{^{1}H}) of the reaction mixtures. As shown in Fig. 2c, the ^{1}H spectrum of the barrel-shaped metallacage **1** exhibited downfield shifts of the characteristic peaks corresponding to aromatic protons ($H_{a\text{-}f,1}$) of coordinated structures, compared with those of pure ligand **3** (Fig. 2b) and di-Pt(II) accepter **4** (Fig. 2d). In addition, the characteristic signals assigned to the aromatic protons (H_a) on the pyridine rings were split into two sets after metal coordination, which was in accordance with the phenomenon in the reported SCC structures [36,37]. Similar trends were also observed in the ^{1}H spectrum of the ball-shaped metallacage **2**, showing the broadening signals with downfield shifts (Figs. 2g, h, and i). The obvious downfield shifts could attribute to the decrease in electron density of original protons brought by the formation of Pt−N coordination bonds. Two-dimensional diffusion-ordered ^{1}H NMR (DOSY) was also performed to provide more evidence for the formation of the simplex assembled products, which exhibit a nearly single vertical trace in both cases. The weight-average diffusion coefficients (D) were measured to be 8.55×10^{-11} m^2/s for the barrel-shaped metallacage **1** (Fig. S24 in Supporting information) and 11.7×10^{-11} m^2/s for the ball-shaped metallacage **2** (Fig. S25 in Supporting information). Moreover, both the ^{31}P{^{1}H} spectra of metallacages, **1** and **2**, exhibited the sharp singlets (*ca.* 16.13 ppm for **1** and 15.11 ppm for **2**) with concomitant ^{195}Pt satellites, which corresponded to a simplex phosphorous environment (Figs. S26 and S27 in Supporting information). The NMR signals of metallacages, **1** and **2**, had pronounced upfield shifts of about 5.78 and 6.19 ppm, respectively, relative to those of precursory Pt(II) acceptors. The well-defined signals in ^{1}H and ^{31}P{^{1}H} spectra of these species supported the formation of the single, discrete assemblies with high symmetry.

The stoichiometry for the formation of discrete metallacages, **1** and **2**, was further supported by observations of electrospray ionization time-of-flight mass spectrometry (ESI-TOF-MS). In the ESI-TOF-MS spectrum of metallacage **1** (Fig. 2e), multiple prominent peaks for $[M - x(OTf)]^{x+}$ ($x = 6–12$) were observed distinctly, which were assigned to the intact [3 + 6] assembly with charge states resulted from the loss of OTf$^-$ counterions (*e.g.*, peak at *m/z* 921.2068 corresponding to $[M - 9OTf]^{9+}$). Similarly, the stoichiometry of discrete metallacage **2** was also evidenced by ESI-TOF-MS (Fig. 2j), which showed ten peaks corresponding to $[M - x(OTf)]^{x+}$ ($x = 7–16$), including the peak at *m/z* 1429.1384 for $[M - 12OTf]^{12+}$. All the relevant peaks were isotopically resolved and in good agreement with their calculated theoretical distributions, suggesting the molecular structure of two discrete metallacages.

In consideration of the difficulty in growing single crystals of these two assemblies suitable for X-ray diffraction, molecular simulations were conducted to afford a further understanding of the structural features of two TPE-containing metallacages, **1** and **2**. All the geometry optimizations were accomplished by exploiting Gaussian09 software in a semiempirical PM6 method. The molecular simulations demonstrated a well-defined barrel-like structure for **1** with a *ca.* 1.6 × 2.5 × 1.1 nm cavity (Figs. 3a and b), while the simulated structure of **2** adopted a ball-like shape possessing a

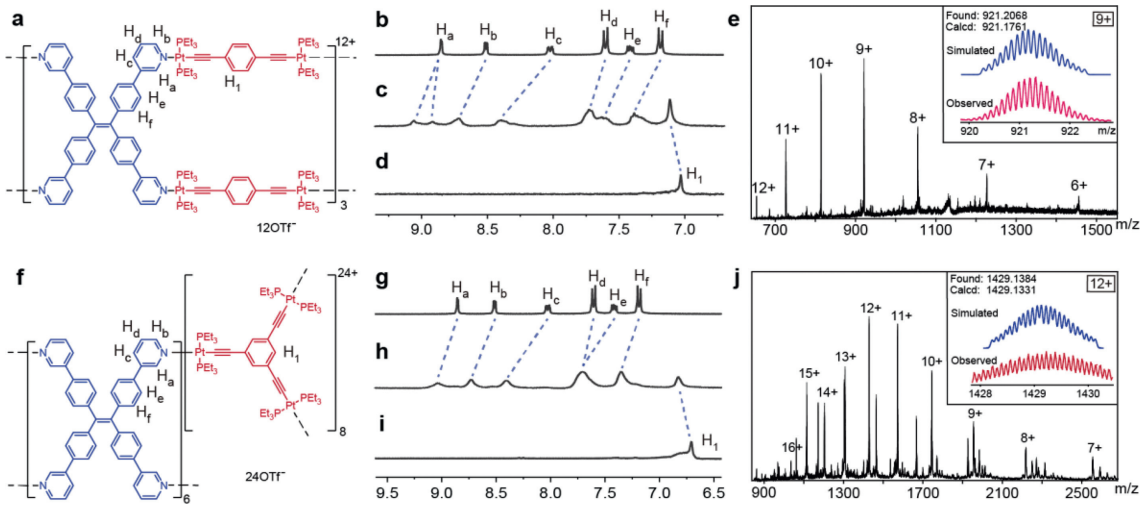

Fig. 2. Simplified chemical structures of metallacages **1** (a) and **2** (f). Partial ^{1}H NMR spectra (400 MHz, DMSO–d_6, 298 K) of ligand **3** (b, g), acceptor **4** (d) and **5** (i) as well as metallacages **1** (c) and **2** (h). ESI-TOF-MS spectra of metallacages **1** (e) and **2** (j).

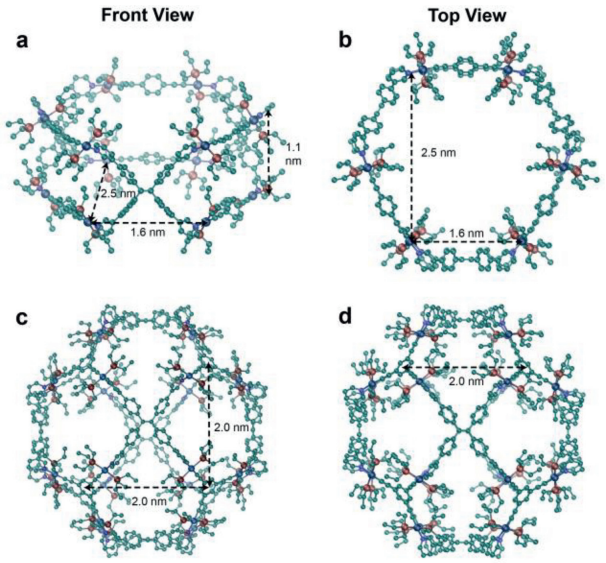

Fig. 3. Ball-and-stick models of the optimized structures of metallacages **1** (a and b) and **2** (c and d). Green balls represent carbon atoms, blue balls represent nitrogen atoms, brown balls represent phosphorus atoms, and gray balls represent platinum atoms.

ca. 2.0 × 2.0 × 2.0 nm cavity (Figs. 3c and d). It is plausible that the ball-shaped metallacage with a closed-framework exert higher tension on TPE units compared to the barrel-shape structure with an open-framework. Such results indicated the ball-shaped assembly might have a stronger restriction on the freedom and flexibility of TPE ligands than the barrel-shaped structure, thereby leading to the different photophysical properties (*vide infra*).

To investigate the photophysical behaviors of the two metallacages, we first recorded the absorption and emission profiles in dilute dichloromethane solutions. In the normalized UV–vis absorption spectra (Fig. 4a), the TPE-based ligand **3** exhibited two broad absorption bands centered at *ca.* 310 and 345 nm, respectively. After metal coordination, the barrel-shaped metallacage **1** only displayed one sharp absorption band at *ca.* 310 nm, while the broad absorption bands of ball-shaped metallacage **2** were centered at *ca.* 325 nm and 345 nm. In the corresponding fluorescence spectra (Fig. 4b), ligand **3** was weakly emissive at *ca.* 525 nm. On the contrary, two metallacages exhibited prominent fluorescence on account of the efficient suppression of TPE units within the rigid metallacage frameworks. Moreover, the emission maximum of barrel-shaped metallacage **1** blueshifted to 515 nm, and the ball-shaped metallacage **2** further blueshifted to 500 nm. According to the TPE-based AIE mechanism, certain wavelength shifts are typically related to specific conformations of the phenyl rings, where a coplanar conformation results in a red shift and a perpendicular conformation leads to a blue shift. The cage tension exerted on TPE units makes the phenyl rings more constrained and perpendicular than the original conformation. It is plausible that the ball-shaped metallacage **2** imposes more constraint on TPE units, thereby causing a more salient blue shift.

It is noteworthy that the ball-shaped metallacage **2** exhibited higher fluorescence intensity compared to the barrel-shaped metallacage **1**. Therefore, we further demonstrated the quantum yields (Φ_F) of the two metallacages in dilute dichloromethane solutions (Figs. S28 and S29 in Supporting information). As expected, the Φ_F of **1** was only 3.47%, and that of **2** was increased to 8.34% (Fig. 4c). Since the enhanced fluorescence resulted from the restriction of TPE units in essence, the more enhanced emission of ball-shaped metallacage was due to higher cage tension of the sphere geometry.

To gain further insight into the AIE properties of the two metallacages with different geometries, the fluorescence spectra were recorded in CH_2Cl_2/hexane mixtures (Figs. 5a and b). The addition of hexane into the CH_2Cl_2 solution could reduce the solubility of the metallacage and thus favor the formation of aggregation. With the increase of the hexane content, the fluorescence intensities were chronologically enhanced and finally reached a maximum at 90% hexane content. Such a phenomenon was consistent with classical AIE behavior, indicating the further restriction of the intramolecular motions of the embedded TPE units upon aggregation. Notably, in the aggregated states when the hexane content reached 90%, a 6.7-fold fluorescence enhancement was observed for the barrel-shaped assembly **1** (Fig. 5c), whereas ball-shaped **2** displayed only a 2.3-fold enhancement (Fig. 5d). In other words, the barrel-shaped scaffold showed a higher fluorescence intensity relative to the ball-shaped one in the aggregated states, which is opposite to what was observed in dilute solutions. This is likely due to greater rigidity as well as tension exerted on TPE units of the spherical structure. In contrast, the bulk sphere scaffold hindered the approach of aggregation in concentrated solutions, thereby showing less amplification. In addition, we observed various yet tunable emissions in different solvents due to the synergis-

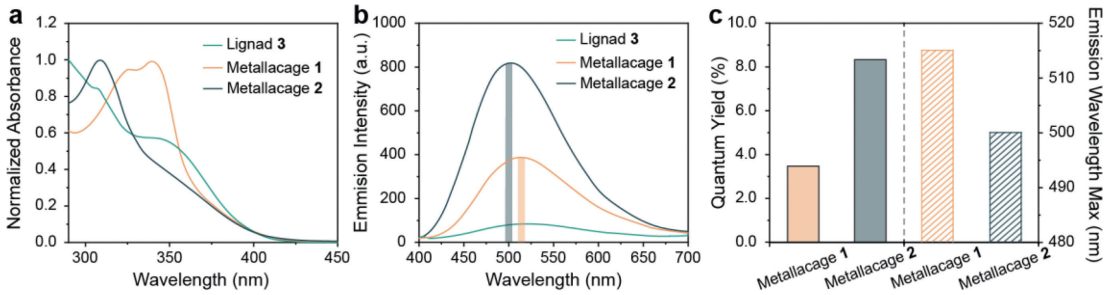

Fig. 4. Absorption (a) and fluorescence (b) spectra of ligand **3**, metallacages **1** and **2** in CH_2Cl_2 (λ_{ex} = 360 nm, c_{TPE} = 10 μmol/L). In view of the metallacages **1** and **2** possessing different amounts of TPE units in the single structure, all photophysical tests were performed by maintaining the identical concentrations of fluorescent TPE units, namely c_{TPE}, of metallacages **1** and **2**. (c) Quantum yield and maximum emission wavelength of metallacages **1** and **2** in CH_2Cl_2 (λ_{ex} = 360 nm, c_{TPE} = 10 μmol/L).

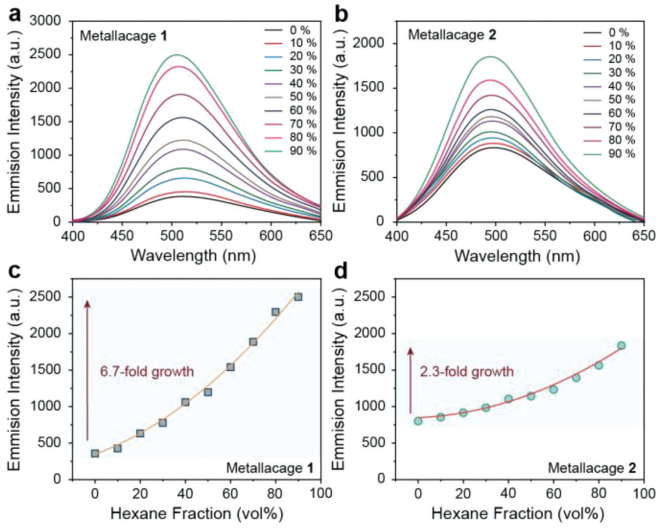

Fig. 5. Fluorescence spectra of metallacages **1** (a) and **2** (b) *versus* hexane fraction in CH_2Cl_2/hexane mixed solutions (λ_{ex} = 360 nm, c_{TPE} = 10 μmol/L). Plots of maximum emission intensity of metallacages **1** (c) and **2** (d) *versus* hexane fraction in CH_2Cl_2/hexane mixed solutions.

tic effect of solubility and polarity. The intensity and wavelength of two metallacages can be readily modulated by simply varying the solvents (Fig. S30 in Supporting information).

In conclusion, we describe the synthesis of emissive barrel-shaped metallacage **1** and ball-shaped metallacage **2** through the stoichiometric and structural control of the same donor and different acceptors. Two metallacages were fully characterized by multinuclear NMR and ESI-TOF-MS for structural confirmation. Due to the differences in the strength and rigidity of the scaffold, as imposed by their shapes, different fluorescence enhancement behaviors were observed. In particular, the barrel-shaped metallacage **1** showed a weaker fluorescence in dilute solutions relative to that of the ball-shaped **2**, while exhibiting a more salient increasing amplitude in the aggregation process. Such a phenomenon demonstrates that the properties of SCCs could be greatly influenced by their geometries, as the more constrained geometry would result in more salient fluorescence. Our work not only enriches the family of light-emitting SCCs, but also enhances the understanding of the mechanism of AIE moieties, thereby providing enlightenment for the novel design of emissive materials.

Declaration of competing interest

The authors declare that they have no known competing financial interests or personal relationships that could have appeared to influence the work reported in this paper.

Acknowledgments

This work was financially supported by Interdisciplinary Program of Shanghai Jiao Tong University (No. YG2019QNA16), Shanghai Sailing Program (No. 20YF1422600), Natural Science Foundation of Shanghai (No. 22dz1207603), and National Natural Science Foundation of China (Nos. 32101092 and 21901161).

Supplementary materials

Supplementary material associated with this article can be found, in the online version, at doi:10.1016/j.cclet.2023.108531.

References

[1] A. Bessette, G.S. Hanan, Chem. Soc. Rev. 43 (2014) 3342–3405.
[2] V.W.W. Yam, V.K.M. Au, S.Y.L. Leung, Chem. Rev. 115 (2015) 7589–7728.
[3] L. Zhang, Y.F. Wang, M. Li, Q.Y. Gao, C.F. Chen, Chin. Chem. Lett. 32 (2021) 740–744.
[4] H. Sepehrpour, W. Fu, Y. Sun, P.J. Stang, J. Am. Chem. Soc. 141 (2019) 14005–14020.
[5] M. Li, S. Jiang, Z. Zhang, et al., CCS Chem. 2 (2020) 337–348.
[6] W. Qian, M. Zuo, P. Niu, X.Y. Hu, L. Wang, Chin. Chem. Lett. 33 (2022) 1975–1978.
[7] Y. Hong, J.W.Y. Lam, B.Z. Tang, Chem. Soc. Rev. 40 (2011) 5361–5388.
[8] J. Luo, Z. Xie, J.W.Y. Lam, et al., Chem. Commun. 18 (2001) 1740–1741.
[9] J. Mei, N.L. Leung, R.T. Kwok, J.W. Lam, B.Z. Tang, Chem. Rev. 115 (2015) 11718–11940.
[10] J. Mei, Y. Hong, J.W.Y. Lam, et al., Adv. Mater. 26 (2014) 5429–5479.
[11] Kenry, B.Z. Tang, B. Liu, Chem 6 (2020) 1195–1198.
[12] N. Jiang, Y. Wang, A. Qin, J.Z. Sun, Z.T. Ben, Chin. Chem. Lett. 30 (2019) 143–148.
[13] M. Zhang, M.L. Saha, M. Wang, et al., J. Am. Chem. Soc. 139 (2017) 5067–5074.
[14] J. Guan, R. Wei, A. Prlj, et al., Angew. Chem. Int. Ed. 59 (2020) 14903–14909.
[15] X.Ji Wang, Z. Li, F. Huang, Adv. Mater. 29 (2017) 1606117.
[16] Z. Wei, Z.Y. Gu, R.K. Arvapally, et al., J. Am. Chem. Soc. 136 (2014) 8269–8276.
[17] X. Yan, T.R. Cook, P. Wang, F. Huang, P.J. Stang, Nat. Chem. 7 (2015) 342–348.
[18] M. Zhang, S. Li, X. Yan, et al., Proc. Natl. Acad. Sci. U. S. A. 113 (2016) 11100–11105.
[19] N.B. Shustova, B.D. McCarthy, M. Dincă, J. Am. Chem. Soc. 133 (2011) 20126–20129.
[20] J. Dong, P. Shen, S. Ying, et al., Chem. Mater. 32 (2020) 6706–6720.
[21] Z. Guo, G. Li, H. Wang, et al., J. Am. Chem. Soc. 143 (2021) 9215–9221.
[22] Z. Guo, J. Zhao, Y. Liu, et al., Chin. Chem. Lett. 32 (2021) 1691–1695.
[23] S. Datta, M.L. Saha, P.J. Stang, Acc. Chem. Res. 51 (2018) 2047–2063.
[24] T. Islamoglu, S. Goswami, Z. Li, et al., Acc. Chem. Res. 50 (2017) 805–813.
[25] M. Pan, W.M. Liao, S.Y. Yin, S.S. Sun, C.Y. Su, Chem. Rev. 118 (2018) 8889–8935.
[26] Y. Sun, C. Chen, P.J. Stang, Acc. Chem. Res. 52 (2019) 802–817.
[27] P.J. Stang, B. Olenyuk, Acc. Chem. Res. 30 (1997) 502–518.
[28] Z. Zhou, X. Yan, M.L. Saha, et al., J. Am. Chem. Soc. 138 (2016) 13131–13134.
[29] W. Wang, Y.X. Wang, H.-B. Yang, Chem. Soc. Rev. 45 (2016) 2656–2693.
[30] X. Yan, M. Wang, T.R. Cook, et al., J. Am. Chem. Soc. 138 (2016) 4580–4588.
[31] Y. Li, J. Zhang, H. Li, et al., Adv. Opt. Mater. 8 (2020) 1902190.
[32] X. Yan, P. Wei, Y. Liu, et al., J. Am. Chem. Soc. 141 (2019) 9673–9679.
[33] J. Zhao, Z. Zhou, G. Li, P.J. Stang, X. Yan, Natl. Sci. Rev. 8 (2021) nwab045.
[34] G. Li, Z. Zhou, C. Yuan, et al., Angew. Chem. Int. Ed. 59 (2020) 10013–10017.
[35] Y. Sun, C. Chen, J. Liu, P.J. Stang, Chem. Soc. Rev. 49 (2020) 3889–3919.
[36] X. Yan, H. Wang, C.E. Hauke, et al., J. Am. Chem. Soc. 137 (2015) 15276–15286.
[37] C. Mu, Z. Zhang, Y. Hou, et al., Angew. Chem. Int. Ed. 60 (2021) 12293–12297.